ELSEVIER

Intermetallics 8 (2000) 1215–1224

Intermetallics

www.elsevier.com/locate/intermet

An empirical model for ideal work of adhesion: transition-metal aluminides and silicides

M.H. Yoo *, K. Yoshimi [1]

Metals and Ceramics Division, Oak Ridge National Laboratory, Oak Ridge, TN 37831-6115, USA

Received 1 November 1999; accepted 31 May 2000

Abstract

The role of atomic bonding in the brittle fracture of intermetallic alloys has been assessed theoretically. A simple empirical model is proposed for the ideal work of adhesion, resulting from a rigid-body separation, in terms of four variables, viz. the elastic stiffness constant, the equilibrium interplanar spacing, and two scaling length parameters. The ratio of these two length parameters is assessed based on the available results of ab initio slab-supercell calculations. Ideal cleavage energies and critical stress intensity factors of transition-metal aluminides and silicides are estimated, and the results are discussed by comparing with the available experimental data of brittle fracture. The difference between the proposed model and other models, temperature dependence of surface energies, and an extension of this model for interfacial adhesion are also discussed. © 2000 Elsevier Science Ltd. All rights reserved.

Keywords: A. Aluminides, miscellaneous; A. Silicides, various; B. Anisotropy; B. Fracture stress; E. Physical properties, miscellaneous

1. Introduction

Transition-metal (TM) aluminides and silicides belong to an important class of material systems because of the use of these silicides in microelectronics industry and the aluminides for possible applications as structural components. Though these TM aluminides and silicides are potential candidates for structural applications at ultra-high temperatures because of their high melting points, relatively low density and good oxidation resistance, the major drawback has been their intrinsic brittleness at room temperature [1,2]. In order to better understand the brittle fracture behavior in silicides of the noncubic crystal structures at low temperatures, specific surface energies of low index habit planes are needed. The purpose of this work is to introduce an empirical method of estimating orientation-dependent uniaxial cohesive energies, or ideal cleavage energies, for TM aluminides and silicides. A brief description of this empirical method was introduced in a recent conference [3].

Experimental data on surface energies of TM aluminides and silicides are not available [4]. A number of different empirical methods have been proposed to correlate surface energies with physical properties such as the heat of fusion, Debye temperature, and the melting point [5,6]. These methods, however, cannot furnish information on the dependence of surface energies on crystallographic planes. On the other hand, electronic structure calculations can give quantitative description on the orientation dependence of surface energy in metals [6–11]. By using the so-called slab model, i.e. free-standing thin film, surface energies of a number of low-index planes in some TM aluminides and silicides were determined by ab initio calculations within the framework of the local density functional (LDF) theory, e.g. in Ni_3Al [12], Ni_3Si [13], TiAl [14], Ti_3Al [15], and $CoSi_2$ [16]. In Al_3Sc [17], NiAl and FeAl [18], and $MoSi_2$ [19], the maximum tensile stresses (or theoretical strength) and uniaxial cohesive energies (or ideal work of adhesion) of a few low-index habit planes were determined as functions of the separation distance by using the so-called supercell model. While most of the experimental techniques to measure surface energies are

* Corresponding author. Tel.: +1-865-574-5165; fax: +1-865-574-7659.

E-mail address: yoo@ornl.gov (M.H. Yoo).

[1] Present address: Institute for Materials Research, Tohoku University, Sendai 980-8577, Japan.

0966-9795/00/$ - see front matter © 2000 Elsevier Science Ltd. All rights reserved.
PII: S0966-9795(00)00082-0

applicable at relatively high homologous temperatures, such as zero-creep technique, theoretical calculations refer to surface energies at the ground state. Therefore, any information on the temperature dependence of surface energies would be useful in comparing the results from theory and experiment.

In this paper, we first present an empirical method of estimating ideal cleavage energies on the basis of the available results of supercell calculations. Second, ideal cleavage energies of TMs and TM aluminides and silicides of cubic and noncubic crystal structures are estimated, and these are compared with the data available in the literature. Third, we discuss temperature and composition dependence of cleavage energies. Finally, the validity and usefulness of the proposed method are discussed in light of the available experimental data and other methods of approximation for surface energy.

2. Uniaxial cohesive stress function

Consider a crystalline slab as illustrated in Fig. 1(a) where the open arrows indicate the direction of uniaxial tensile stress, σ, as a function of the displacement, v, along the y-axis. The three material-specific length parameters of d_0, a, and D represent the equilibrium interplanar spacing of (hkl) planes, an effective range of interatomic cohesive forces, and a scaling factor related to the nonlinear nature of $\sigma(v)$, respectively. The change in total energy of a slab, ΔE, as it is separated into two halves, is to increase with increasing separation distance, v, as shown in Fig. 2(a). The corresponding tensile stress function is shown in Fig. 2(b) such that the ideal cleavage energy is obtained by

$$G_c = \int_0^\infty \sigma(v)\mathrm{d}v = \gamma_1 + \gamma_2 \tag{1}$$

where γ_1 and γ_2 are the specific energies per unit area of the two surfaces created, as indicated in Fig. 1(b). In

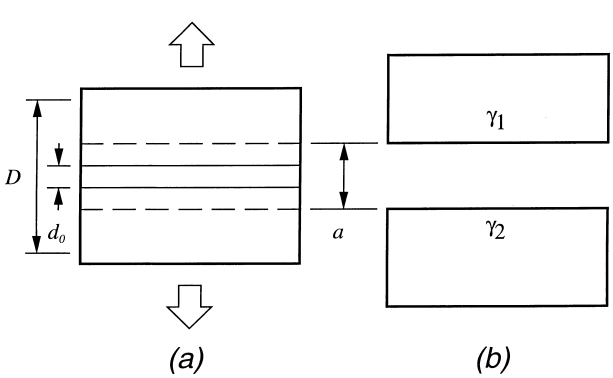

Fig. 1. Schematic illustration of (a) a supercell unit and (b) two parts after separation.

ordered intermetallic compounds, these two surface energies are equal only at some special crystallographic orientations. In addition, for some (hkl) planes in noncubic crystals, there are more than one choice of atomically distinct cleavage plane.

If the cohesive stress function, $\sigma(v)$, is known, then the ideal cleavage energy (work of adhesion) can be obtained from Eq. (1). But, in reality, it is the change in total energy as a function of separation distance, $\Delta E(v)$, that can be calculated by a supercell calculation. This result becomes then the basis for constructing the stress function, $\sigma(v)$. The so-called universal binding energy relation (UBER) [20,21], which is known valid for metallically and covalently bonded solids, can be used to fit the ΔE–v data of supercell calculations by

$$\Delta E(v) = G_c[1 - (1 + d^*)\exp(-d^*)], \tag{2}$$

where d^* is defined in terms of a scaling length (or the electronic screening length [20]), l, as $d^* = v/l$. The uniaxial tensile stress function is given by

$$\sigma(v) = \sigma_m d^* \exp(1 - d^*). \tag{3}$$

The peak tensile strength and the cleavage energy are related to each other simply by [22]

$$G_c/\sigma_m = el, \tag{4}$$

where e is the base of natural logarithm. The interfacial energy results of supercell calculations for (001) planes in Mo, Nb, V, and $MoSi_2$ were found to fall accurately on a single UBER curve when the scaling length is in the range of $l = 0.63$–0.70 Å [19].

In this paper, we are interested in the anisotropy of cleavage energy for a given TM aluminides or silicide. In using a triangular approximation for the stress function in Fig. 2(b), we assume that (i) the maximum slope of the ΔE–v curve (i.e. $\sigma = \sigma_m$) occurs at $v = l$, (ii) at $v < l$, the nonlinear $\sigma(v)$ is approximated by the reduced elastic stiffness of $C_{22}(d_0/D)$ in the direction perpendicular to (hkl) planes, and (iii) the long-range interatomic forces (at $v > l$) diminish effectively to zero at $v \geqslant a$. On the basis of these three assumptions, the tensile cohesive stress may be given simply as

$$\sigma = C_{22}\left(\frac{v}{D}\right) \qquad \text{for } 0 \leqslant v \leqslant l, \tag{5a}$$

$$\sigma = \frac{C_{22}}{D}\left(\frac{l}{a-l}\right)(a - v) \qquad \text{for } l < v \leqslant a, \tag{5b}$$

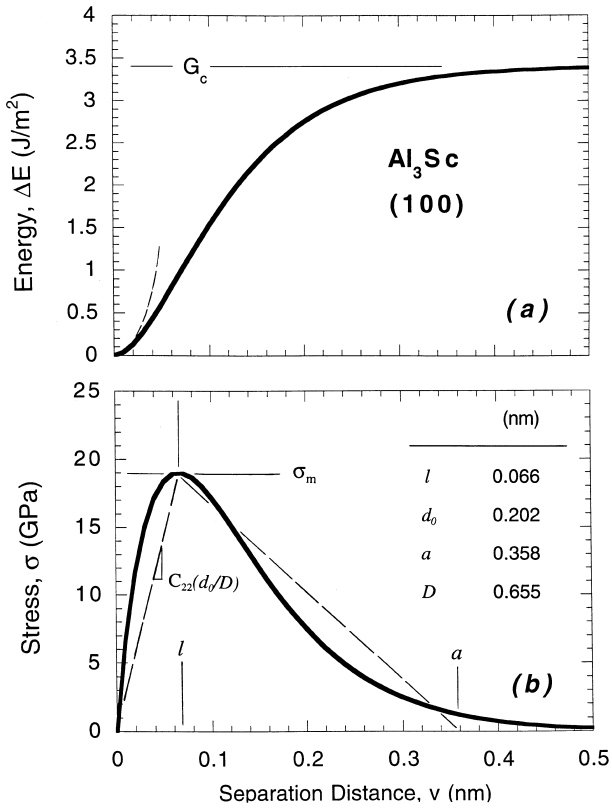

Fig. 2. (a) Interfacial energy and (b) tensile stress for the (100) plane in Al_3Sc based on the ab initio supercell calculations [17].

$$\sigma = 0 \qquad \text{for } v > a, \tag{5c}$$

where C_{22} is the transformed elastic stiffness constant with respect to the tensile y-axis. Use of the above stress function based on the three assumptions and Eq. (1) gives the maximum stress and the cleavage energy as

$$\sigma_m = C_{22}\left(\frac{l}{D}\right), \tag{6}$$

$$G_c = \frac{C_{22}l}{2}\left(\frac{a}{D}\right). \tag{7}$$

Eq. (6) for the ideal cleavage strength is equivalent to a number of such expressions [23–26] based on the original Orowan–Polanyi approximation for the theoretical tensile strength. The elastic stiffness constants in place of Young's modulus were used earlier for the case of hcp metals [27]. The dashed curve of Fig. 2(a) is the harmonic range of the energy increase corresponding to the elastic constant C_{22}. The Orowan–Polanyi approximation usually makes an overestimate of the theoretical strength in metals. For instance, in the case of TM aluminides, the estimated cleavage strength in the range of $\sigma_m = (0.12–0.18)\ C_{22}$ was found to be slightly larger than those determined from the slab-supercell calculations [14]. The proposed triangular approximation is designed to match the maximum stresses determined from supercell calculations by use of the D parameter, which may be related to the anharmonic property at the "bond-stretching" part ($v < l$) of Fig. 2.

The area under a triangular stress function is chosen exactly the same as that under a $\sigma(v)$ curve, as illustrated in Fig. 2(b) by the two dashed lines in compliance with the solid curve. According to the prescription of scaling for the UBER [20,21], σ_m occurs at $v = l$. The supercell calculations for TM aluminides [17,18] showed that ΔE converges to different G_c values for different cleavage habit planes. Therefore, the parameter a, which is related to the "bond-breaking" part ($v > l$) of Fig. 2, is to be correlated not only to the actual magnitude of cleavage energy for a given compound, but also to the anisotropy of cleavage energy in the compound. This parameter has a simple relationship with the scaling length, l,

$$\frac{a}{l} = 2e. \tag{8}$$

Use of this in Eq. (7) gives an alternative expression of cleavage energy,

$$G_c = eC_{22}\left(\frac{l^2}{D}\right). \tag{9}$$

3. Determination of length parameters

In this section, the length parameters involved in the triangular approximation are determined for three bcc metals (Mo, V, and Nb), two B2 aluminides (NiAl and FeAl), two $L1_2$ aluminides (Al_3Sc and Ni_3Al), and one $C11_b$ silicide ($MoSi_2$).

Fig. 3 and Table 1 summarize the supercell calculations for (001) cleavage in Mo, V, Nb, and $MoSi_2$ by Hong et al. [19]. In Tables 1–3, numerical factors of $\lambda = l/d_0$ are listed. $MoSi_2$ has the tetragonal $C11_b$ structure, which consists of three pseudo-bcc unit cell stacked along the [001] direction. The data of $MoSi_2$ are referred to fracture between the Si (001) plane, and hence $G_c = 2\gamma$.

Fig. 4 and Table 2 summarize the results of supercell calculations for NiAl and FeAl reported by Yoo and Fu [18]. In an AB compound of the B2 structure, one of the (100) cleavage surfaces consist of all A atoms and the other with all B atoms, accordingly, $G_c = \gamma_1 + \gamma_2$. In contrast, all {110} surfaces being equal in the A + B composition, we have $G_c = 2\gamma$ for the case of (110) cleavage in stoichiometric B2 compounds.

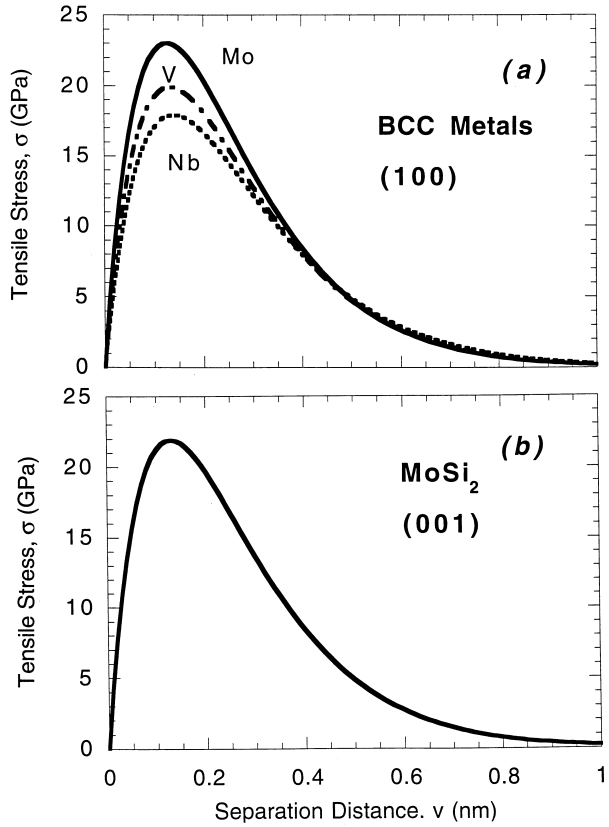

Fig. 3. Tensile stress vs. cleavage displacement in (a) bcc TM metals and (b) $MoSi_2$ based on the ab initio supercell calculations [19].

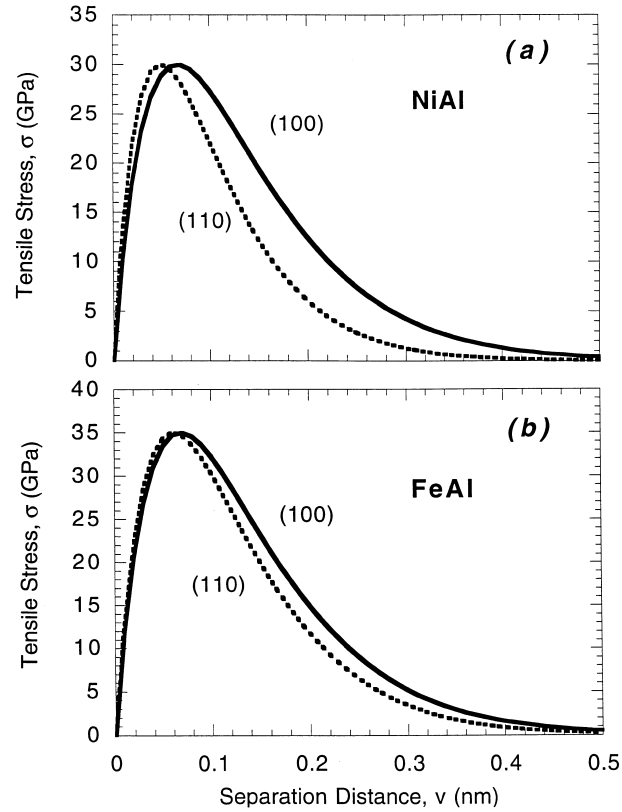

Fig. 4. Tensile stress vs. cleavage displacement in (a) NiAl and (b) FeAl based on the ab initio supercell calculations [18].

Table 3 lists the data for Al_3Sc [17] and Ni_3Al [12] of the $L1_2$ structure. Cleaving on (100) or (110) plane of an A_3B crystal of the $L1_2$ structure creates two surfaces of different chemical composition, one containing all A atoms and the other of A + B atom mixture. Therefore, $G_c = \gamma_1 + \gamma_2$ for both cases. The $\sigma(v)$ curves for Al_3Sc and Ni_3Al are very similar in shape to Fig. 4(b) and 2(b), respectively, with an exception that the (100) curve is slightly lower than the (110) curve in Al_3Sc.

Table 4 summarizes all the length parameters involved in Eqs. (6), (7), and (9). The elastic constants used for metals are from the experimental data either at

Table 1
Ideal work of fracture, theoretical strength, and length parameters for (001) cleavage in the BCC case [19]

Metals	(*hkl*)	G_c (J/m^2)	σ_m (GPa)	d_o (nm)	l	λ
Mo	200	7.94	23.0	0.157	0.063	0.404
V	200	7.20	19.9	0.152	0.067	0.438
Nb	200	6.82	17.9	0.165	0.070	0.425
$MoSi_2$	006	7.72	21.9	0.131	0.065	0.495

Table 2
Ideal work of fracture, theoretical strength, and length parameters in the B2 case [18]

Aluminides	(*hkl*)	G_c (J/m^2)	σ_m (GPa)	d_o (nm)	l	λ
NiAl	200	5.5	30	0.141	0.067	0.478
	110	4.1	30	0.199	0.050	0.253
FeAl	200	6.5	35	0.142	0.068	0.481
	110	5.8	35	0.200	0.061	0.348

Table 3
Ideal work of fracture, theoretical strength, and length parameters in the $L1_2$ case [12,17]

Aluminides	(*hkl*)	G_c (J/m^2)	σ_m (GPa)	d_0 (nm)	l	λ
Al_3Sc	200	3.4	19	0.202	0.066	0.326
	110	3.7	19	0.286	0.072	0.250
Ni_3Al	200	5.8	30	0.175	0.071	0.406

4 K or their extrapolations to 0 K [28]. Unless mentioned otherwise, the elastic constants used for intermetallic compounds are from the tabulation of theoretical results at the ground state [29]. The elastic constants of NiAl and FeAl are from Fu and Yoo [30]. Among eleven cases representing eight different materials, the numerical value of λ ranges from 0.25 to 0.50, where the low bound is represented by Al_3Sc (110) and the high bound by $MoSi_2$ (006). Among the three bcc metals, the peak stress increases ($\sigma_m = 18$, 20, and 23 GPa for Nb, V, and Mo) while the peak position decreases slightly ($l = 0.70$, 0.67, and 0.63 Å). This increase can be correlated to the increase in the reduced elastic stiffness constant, viz., $C_{22}(d_0/D) = 42$, 45, and 57 GPa for Nb, V, and Mo, respectively.

In the B2 case, cleavage energy of the (110) plane is lower than that of the (100) plane. Though only slight, the anisotropy is opposite in the case of Al_3Sc. The rather pronounced anisotropy of G_c (about 30%) in NiAl, while the $\sigma_m = 30$ GPa is the same, can be correlated to both the a and D parameters. That is, a is larger for the (100) plane than for the (110) plane by 34% and $C_{22}(d_0/D)$ is smaller by a factor of two.

4. Ideal cleavage energy and strength

4.1. Transition metals

Table 5 lists estimated values of (100) cleavage energies for four bcc (Ta, Cr, W, and Fe) and four fcc (Ni, Pd, Pt, and Al) metals. The numerical value of l^2/D used for Ta is the algebraic average of the two values for V and Nb. Two different values of l^2/D (corresponding to Nb and Mo) were used for Fe. Because no supercell calculation database is available for fcc metals, $l^2/D = 0.908 \times 10^{-2}$ determined for Ni_3Al was used for Ni, Pd, and Pt. The two l^2/D values determined for (100) and (110) planes of Al_3Sc were used for the two planes of Al.

The estimated results of G_c by this study are compared with the available results of first-principles slab calculations within the local density approximation (LDA), which are listed in Table 5. Also listed in Table 5 are the predicted values from the so-called equivalent-crystal-theory (ECT) [31] and other values obtained using semi-empirical methods, such as the embedded atom method (EAM) [32] and Finnis–Sinclair method [33]. Except for Pd and Pt [34], all other data of the three columns (LDA, ECT, and Other) in Table 5 are obtained from Table III of Smith et al. [31].

When compared to LDA values, the estimated G_c values for (100) plane in Fe and Ni, and (110) plane in Al are larger by about 6 and 12%, respectively, and the estimated G_c value for (100) plane in W is smaller by about 8%. While the results from ECT are generally larger than the LDA results by about 10% on average, the predictions of G_c values by other semi-empirical methods are 45–55% lower than the LDA results. In the empirical method proposed in this paper, transferring of the l^2/D values from Ni_3Al to Ni and from Al_3Sc to Al

Table 4
Elastic constants and length parameters

Material	(*hkl*)	C_{22} (GPa)	D (nm)	a	$(l^2/D)\times 10^2$	$\frac{D}{d_0}$	$\frac{l}{D}\times 10^2$
Mo	200	450	0.621	0.345	0.649	7.89	5.1
V	200	232	0.389	0.362	1.140	5.13	8.6
Nb	200	253	0.495	0.381	0.993	6.00	14.0
$MoSi_2$	006	536	0.794	0.353	0.530	12.13	4.1
NiAl	200	233	0.524	0.367	0.868	3.73	12.9
	110	318	0.533	0.273	0.474	2.68	9.4
FeAl	200	290	0.566	0.371	0.825	4.00	12.1
	110	375	0.653	0.331	0.569	3.26	9.3
Al_3Sc	200	189	0.655	0.358	0.662	3.24	10.5
	110	182	0.686	0.390	0.748	2.40	10.4
Ni_3Al	200	235	0.557	0.387	0.908	3.19	12.8

Table 5
Estimate of (100) ideal cleavage energy for transition metals and Al

Metals	C_{22} (GPa)	$(l^2/D)\times10^2$ (nm)	This study	LDA	ECT	Other
			G_c (J/m^2)			
V[a]	232	1.140	7.20	7.20[a]		
Nb[a]	253	0.993	6.82	6.82[a]		
Ta	266	1.066	7.72			
Cr	391	0.649	6.90			
Mo[a]	450	0.649	7.94	7.94[a]		
W	533	0.649	9.40	10.20	11.76	5.85
Fe	243	0.649	4.29			
		0.993	6.56	6.20	6.98	3.39
Ni	261	0.908	6.45	6.10	6.24	3.16
Pd	234	0.908	5.78			3.82
Pt	358	0.908	8.84			4.88
Al (200)	116	0.662	2.09		2.58	
(110)	121	0.748	2.47	2.20	2.32	

[a] Database from ab initio supercell calculations [19] available for this study.

is a reasonable exercise in view of the good agreement between the estimated values and the LDA results. Also, the reasonable agreement between the estimated value of $G_c = 6.56$ J/m^2 and the LDA result of $G_c = 6.10$ J/m^2 indicates that Fe is more similar to Nb than to Mo as far as the l^2/D numerical factor is concerned.

4.2. TM aluminides and silicides

In addition to the eight cases of five intermetallic compounds for which all the length parameters were determined (Table 4), there are more data for G_c from *ab initio* slab calculations, from which numerical values of l^2/D can be determined. Table 6 lists these additional data for Al_3Sc [17], Ni_3Al [12], Ni_3Si [13,35], $CoSi_2$ [16], TiAl [14,36], and Ti_3Al [15,36], which contains 12 cases for the six alloys. Together with those cases for alloys listed in Table 4, a total number of cases is 20 for nine alloys.

Using appropriate values of l^2/D from Tables 4 and 6, we can estimate ideal cleavage energies for many TM aluminides and silicides of $L1_2$, $D0_{22}$, $D0_{23}$, B2, $D0_3$, and $C11_b$ structures, as listed in Table 7. Transfer of l^2/D values within the same crystal structure or from one pseudo-fcc (or-bcc) building block to another was made in the following ways: $Ni_3Al \rightarrow Pt_3Al$, $Al_3Sc \rightarrow$ all trialuminides, $(NiAl+FeAl)/2 \rightarrow$ B2 aluminides, FeAl $\rightarrow$ Fe-base $D0_3$ and $MoSi_2 \rightarrow WSi_2$. To our best knowledge, there has been no information on numerical values of G_c for the cases listed in Table 7. The elastic constants used in Table 7 are mostly from experimental data at room temperature [29]. Theoretically determined elastic constants at 0 K were used for Pt_3Al [37], Al_3Ti ($L1_2$) [17], and RuAl and CoAl [38].

Though there is no experimental database for G_c values, a comparison can be made between theoretically-determined Griffith strength and experimentally-measured fracture toughness. Table 8 lists such results for a comparison between $MoSi_2$ and WSi_2. The critical stress intensity factor for mode-I (*hkl*)[*uvw*] Griffith crack, k_{IG}, was determined by taking full account of the elastic anisotropy [13]. The fracture toughness values,

Table 6
Cleavage energy and the ratio of length parameters

Alloys	(*hkl*)	G_c (J/m^2)	C_{22} (GPa)	l^2/D (10^{-2})
Ni_3Al	111	4.6	351	0.482
Ni_3Si	200	7.2	375	0.706
	111	5.1	481	0.390
Al_3Sc	111	3.3	180	0.675
$CoSi_2$	400	5.96	277	0.792
	220	4.62	309	0.550
	222	4.34	320	0.499
TiAl	200	4.6	188	0.900
	002	5.6	190	1.084
	110	5.3	243	0.802
	111	4.5	283	0.585
Ti_3Al	002	4.8	238	0.742

Table 7
Estimate of ideal cleavage energy for TM aluminides and silicides

Alloys	(*hkl*)	C_{22} (GPa)	$(l^2/D)\times10^2$ (nm)	G_c (J/m^2)
Pt_3Al	200	436	0.908	10.8
	111	479	0.482	6.3
Al_3Ti[a]	200	177	0.662	3.2
	110	212	0.748	4.3
	111	224	0.676	4.1
Al_3Ti	200	218	0.662	3.9
	110	254	0.748	5.2
	111	250	0.676	4.6
Al_3Zr	200	209	0.662	3.8
	110	242	0.748	4.9
	111	241	0.676	4.4
RuAl	200	308	0.847	7.1
	110	348	0.522	4.9
CoAl	200	251	0.847	5.8
	110	310	0.522	4.4
Fe_3Al	200	171	0.825	3.8
	110	267	0.569	4.1
Fe_3Si	200	232	0.825	5.2
	110	331	0.569	5.1
$MoSi_2$	110	454	0.522	6.4
WSi_2	110	400	0.522	5.7
	006	552	0.530	8.0

[a] $L1_2$ structure (hypothetical).

K_{IC}, were obtained from three-point bending tests of single crystals [39]. The k_{IG} and K_{IC} values listed in Table 8 indicate that the amount of crack-tip plasticity seems to be relatively larger at (001)[110] crack than at a (110)[001] crack in both WSi_2 and $MoSi_2$. This is more so in $MoSi_2$.

5. Temperature, composition, and interface

We have discussed ideal cleavage energy and strength in terms of four variables (C_{22}, d_0, l or a, and D) that are not only material specific, but also orientation dependent. So far, we have dealt with pure metals and stoichiometric compounds at the ground state and/or room temperature and G_c as the net change in interfacial energy by a rigid-body separation. The role of surface relaxation (or reconstruction) is neglected because it is known to be a minor effect, e.g. less than 2% of the W(100) surface energy and less than 4.5% of the V(100) surface energy [40].

There have been many papers during the 1980s that discuss the physical meaning of the scaling length, l, in the UBER. One possible interpretation is that the first-order anharmonic properties (such as thermal expansion) are related in a simple way to the harmonic properties (bulk modulus). In the present study, the anisotropy of this simple relationship is of primary interest.

For a given (*hkl*) plane how the two length parameters, l and D, change with temperature is not known, but the temperature dependence of G_c due to changes in elastic constants can be assessed. Fig. 5 shows temperature dependence of G_c for the (100) and (110) planes in NiAl by using the elastic constants over a temperature range of 300–1100 K [41]. The change in d_0 values on account of thermal expansion is negligibly small compared to that in elastic constants. The anisotropy of G_c is reduced significantly at higher temperatures, the G_c ratio of (110)/(100) reaching 0.93 at 1100 K, as far as the enthalpy term of surface energy is concerned. Contribution of the surface entropy may become an important factor at high temperatures, e.g. $\Delta S\approx1.5\times10^{-3}$ J/m^2 deg above 1000 K for W (001) surface [40], but such information is not available for intermetallic compounds.

Using the elastic constants of Al-rich TiAl [42], we find the temperature dependence of G_c as shown in Fig. 6. Because of the difference in elastic constants between the calculated results for stoichiometric TiAl at 0 K [38] and the experimental data on Ti–56% Al at 300–750 K [42], G_c values of the (110) and (111) planes in Fig. 6 are lower than the corresponding values in Table 6 by 11 and 13%, respectively. Thus, Fig. 6 actually represents a combined effect of temperature and hyperstoichiometry on G_c through elastic constants. The anisotropy of thermal expansion coefficients [42] is too small to make any appreciable change in the axial ratio ($c/a=1.02$). With an exception of the (100) curve, the three curves in Fig. 6 show essentially the same temperature dependence.

In many intermetallic compounds, elastic constants are known to be strongly composition dependent, e.g. Ni–Al and Fe–Al systems [43,44]. In both systems, the elastic anisotropy increases as a binary compound becomes more TM-rich. Consequently, the difference in G_c between (100) and (110) planes in a hypostoichiometric

Table 8
Cleavage energy, Griffith strength, and fracture toughness of $C11_b$ TM disilicides [39]

Disilicides	(*hkl*)	G_c (J/m^2)	[*uvw*]	k_{IG}	K_{IC}
				(MPa$-\sqrt{m}$)	
WSi_2	006	8.0	110	2.0	3.7
	110	5.7	001	1.6	3.1
$MoSi_2$	006	7.7	110	1.9	4.0
	110	6.4	001	1.7	2.4

NiAl alloy (e.g. > 54% Ni) is expected to be much larger than that shown in Fig. 5. It is not known, however, how l and D or l^2/D are affected by a high concentration of intrinsic point defects.

In the case of two-phase TiAl–Ti_3Al alloys containing γ/γ and α_2/γ interfaces, the interfacial cleavage energies can be estimated by

$$G_i = G_c - \Gamma_i - E_m \tag{10}$$

where Γ is the interfacial energy and E_m is the misfit energies based on Frank and van der Merwe method [45]. Because of the approximations involved in determining the interfacial and misfit energies, the interfacial fracture energies obtained earlier [36,46] are only estimates. Nevertheless, the results showed that interfacial fracture is more likely to occur on an 120° rotational γ/γ boundary than on the α_2/γ boundary. Use of $G_c = 4.5$ J/m^2 for TiAl (111) and $G_c = 4.8$ J/m^2 for Ti_3Al from Table 6 brings another degree of approximation because, in reality, both γ and α_2 phases are off-stoichiometric in their chemical compositions.

6. Discussion

On the total of 25 cases for three metals and nine alloys, for which the results of G_c by ab initio slab-supercell calculations are available in the literature, a systematic analysis of correlation between G_c and l^2/D was made based on the proposed triangular approximation for the cohesive stress function. Transfer of l^2/Ds from one bcc TM to another was made directly within the isoelectronic VA and VIA groups. Whereas, for fcc TMs and Al, the l^2/D values of Ni_3Al and Al_3Sc were used, respectively. In the case of TM aluminides and silicides, transfer of l^2/D from one crystal class to another within a given chemical group (mono-aluminides, monosilicides, trialuminides, or disilicides) was made by comparing pseudo-fcc and pseudo-bcc building blocks of cubic and noncubic crystal structures. Then, estimate of G_c was made for a total of eight metals (4 bcc and 4 fcc) and for 22 cases for 10 intermetallic compounds.

The lowest cleavage energy among the total of 43 cases is $G_c = 3.3$ J/m^2 for (111) plane of Al_3Sc (Table 6). In other trialuminides, essentially isotropic C_{22} and a moderate variation of l^2/D in Al_3Sc give the lowest G_c for (100) planes in both $TiAl_3$ and $ZrAl_3$ (Table 7). Relatively low cleavage energies ($G_c \leqslant 5$ J/m^2) of trialuminides stem directly from the high coordination of Al atoms. The highest cleavage energy is the estimated value of $G_c = 10.8$ J/m^2 for Pt_3Al (100), which is comparable to the LDA and ECT values for W listed in Table 5. It can be seen also in Table 5 that Pt has the highest (100) G_c value among the fcc TMs in the VIIIA group. When (100) and (111) G_c values are compared, these are larger for Pt_3Al than for Ni_3Al by factors of 1.9 and 1.4, respectively, which are due to the substantially larger elastic stiffness constants of Pt_3Al than of Ni_3Al.

The magnitude and anisotropy of G_c of RuAl are larger than those of CoAl and NiAl (Table 7). The estimates of (100) G_cs for Fe_3Al and Fe_3Si are lower than the calculated values of FeAl (Table 2) and the estimated value for Fe (Table 5) by 42 and 20%, respectively. Again, according to Eq. (6) or (9), these differences are due to the differences in C_{22} values.

When a cleaving interface creates two different surfaces, the range of interatomic interaction is estimated to be more long-range compared to the case when the two surfaces are chemically the same. A comparison of {100} planes to more close-packed {110} planes in bcc-based B2 aluminides (Table 2) is a case in point. Similarly, we notice such correlation between {100} and {111} in $L1_2$ aluminides and silicide (Tables 3 and 6), and also between (001) and (111) in TiAl (Table 6).

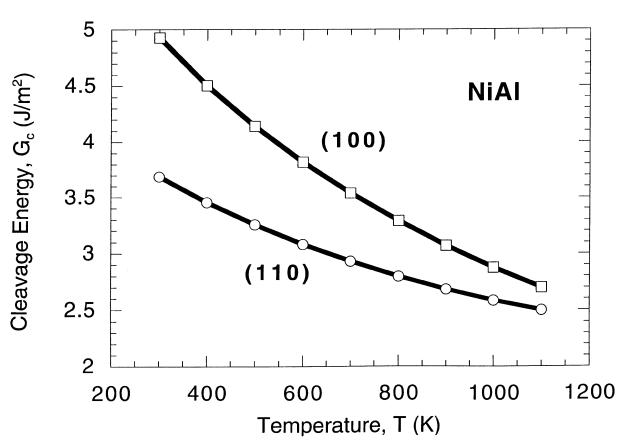

Fig. 5. Temperature dependence of cleavage energies in NiAl based on the change in elastic constants [41].

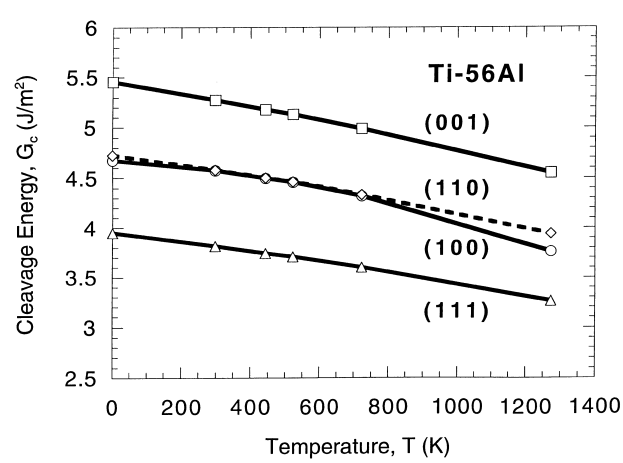

Fig. 6. Temperature dependence of cleavage energies in TiAl based on the change in elastic constants [42].

Along the close-packed (nearest-neighbor) direction, strong directional bonding between TM and Al or Si arises from the combination of charge transfer and strong p (Al or Si)–d (TM) hybridization effect [30,47].

The difference in magnitude and anisotropy of G_cs between Ni_3Si and Ni_3Al can be discussed in terms of an extra p-electrons in Ni_3Si [13], which raises the magnitude of C_{22}. Analogously, the two higher G_cs and the anisotropy in Fe_3Si as compared with Fe_3Al (Table 7) can be attributed to the role of an extra p-electron in increasing the interatomic interaction in Fe_3Si, more across the (100) plane than across the (110) plane. This is consistent with the differences in C_{22} on these two planes between Fe_3Si and Fe_3Al, i.e. C_{22} on (100) increases by 36% while C_{22} on (110) increases by 17%. In terms of G_c alone, both Ni-base and Fe-base silicides are intrinsically less brittle than the corresponding aluminides. The reason for much higher fracture toughness measured in the aluminides is obviously related to the role of crack-tip plasticity.

The present model based on a triangular approximation for cleavage strength and energy has the following relationships with other models. The first and second assumptions of the present model give an expression for the ideal cleavage strength, Eq. (6), where $\varepsilon = l/D$ can be called the "maximum elastic strain" or the "elastic limit." The magnitude of this strain in the range of $4\% < l/D < 14\%$ (Table 4) is somewhat lower than $\epsilon \approx 1/10$ [24] and $\epsilon \approx 1/\pi$ [23] estimated on the basis of the Orowan–Polanyi approximation. As shown by Eq. (8), the a parameter is larger than the l parameter of the UBER by a factor of 5.44. The so-called four point model of UBER [19] is capable of estimating ideal cleavage stresses, for a given surface orientation, without resorting to any more than four supercell calculations. The model proposed here introduces the elastic stiffness constant as one of the four variables in such a way that the combined length parameter (l^2/D), together with C_{22}, can be used to approximately describe the anisotropy of cleavage energy.

As in the case of bcc and fcc TMs discussed earlier (Table 5), the G_c values of B2 and $L1_2$ intermetallics estimated using the EAM interatomic potentials are generally lower than those given by LDA calculations. For instance, as compared to the G_c values listed in Table 2, those for (100) and (110) surfaces in NiAl estimated by Ludwig and Gumbsch [48] are lower by 36 and 33%, respectively, and the G_c values given by Farkas [49] are lower by 28 and 17%. In Ni_3Al, Foiles and Daw [50] estimated $G_c = 3.51$ and 3.30 J/m^2 for (100) and (111) surfaces, respectively, which are lower than the corresponding G_c values in Tables 3 and 6 by 39 and 28%. The reason for these large discrepancies are not known.

Experimental data on cleavage habit planes are scarce, but the available information is generally consistent with the calculated G_c values in Tables 1–3 and 6 as was discussed earlier [13,15,18]. In Al_3Sc, the main fracture surface was observed to be {110} plane [51], which is not in accord with the G_c values listed in Tables 3 and 6. This indicates that the anisotropy in crack-tip plasticity by slip and twinning is the controlling factor, particularly in the so-called "soft and brittle" compounds. In the study of fractured surfaces based on the selected area electron channeling patterns, George et al. [52] concluded that the availability of several low-strength cleavage planes in an Al–23Ti–6Fe–5V polycrystalline alloy apparently exacerbates its brittleness. On the other hand, the estimate of $G_c = 3.7$ J/m^2 being the lowest in $TiAl_3$ (Table 7) is consistent with the transmission electron microscopy observation of {100} habit plane in Al–25Ti–8Cr single crystals [53].

Fracture toughness of $MoSi_2$ at room temperature has been estimated by examining the cracks around a hardness indenter [54,55]. The estimated data are 3 MPa-$\sqrt{m}$ in polycrystals [54] and 4 MPa-$\sqrt{m}$ for (001) < 100 > cracks in single crystals [55]. As was discussed by referring to Table 8, in intrinsically brittle materials such as $MoSi_2$ and WSi_2, anisotropic G_c values and fracture toughness data from single crystals can be used together to assess the relative role of crack-tip plasticity. It may be concluded from the results in Table 8 that in $MoSi_2$ the amount of crack-tip plasticity appears to be larger at a (001)[110] crack, $(K_{IC} - k_{IG})/k_{IG} = 1.1$, than at a (110)[001] crack, 0.3, by a factor of more than three. The transmission electron microscopy investigation by Ito et al. [39] revealed stacking faults of the Frank-type on (001) which are formed probably due to the loss of silicon during high-temperature exposure. These faults, which are more abundant in WSi_2 than in $MoSi_2$, may contribute also to the difference and the anisotropy of fracture toughness in these two TM disilicides.

As we consider tougher and stronger silicides of ultra-high melting temperatures, which have mostly noncubic crystal structures, the anisotropy of G_c remains a very important factor in describing their integrity after processing and handling.

7. Summary

A simple expression for the ideal work of adhesion, resulting from a rigid-body decohesion of a (hkl) plane, is proposed in terms of four variables, viz. the elastic stiffness constant, the interplanar spacing, and two scaling length parameters (D and a or l). By using the available results of ab initio slab-supercell calculations, the anisotropy of l^2/D is assessed. Within a chemical group, the ideal cleavage energies of TM aluminides and silicides were estimated by comparing pseudo-fcc and pseudo-bcc building blocks of cubic and tetragonal crystals.

Acknowledgements

The authors would like to thank C.L. Fu, J.A. Horton, and E.P. George for stimulating discussions and helpful comments on the manuscript. This research was sponsored by the Division of Materials Sciences and Engineering, Office of Basic Energy Sciences, US Department of Energy, under Contract DE-AC05-00OR22725 with UT-Battelle, LLC, and also supported in part by the program of Japan Society for the Promotion of Science Postdoctoral Fellowships for Research Abroad.

References

[1] Bewlay BP et al., editors. High-temperature silicides and refractory alloys. Pittsburgh Symp. Proc., vol. 322, Pittsburgh (PA): MRS, 1994.
[2] Petrovic JJ et al., editors. High temperature structural silicides. Abstract Bulletin of Engineering Foundation Conference, 25–29 May 1998, Hyannis, MA.
[3] Yoo MH, Yoshimi K. In: George EP et al., editors. High-temperature ordered intermetallic alloys VIII. Symp. Proc., vol. 552. Pittsburgh (PA): MRS, 1999. p. KK6.6.1.
[4] Murr LE. Interfacial phenomena in metals and alloys. Reading: Addison-Wesley (MA), 1975.
[5] Grimvall G, Sjödin S. Physica Scripta 1974;10:340.
[6] Lang ND, Kohn W. Phys Rev, B1:4555
[7] Harris J, Jones RO. Phys Lett 1974;46A:407.
[8] Rose JH, Smith JR, Ferrante J. Phys Rev Lett 1981;47:675
[9] Smith JR, Rose JH, Ferrante J, Guinea F. In: Langreth D et al., editors. Many-body phenomena at surfaces. New York: Academic, 1984. p. 159–174.
[10] Methfessel M, Henning D, Scheffler M. Appl Phys 1992;A55:442.
[11] Mehl MJ, Papaconstantopoulos DA. Phys Rev 1996;B54:4519.
[12] Fu CL, Yoo MH. In: Liu CT et al., editors. Ordered intermetallics — physical metallurgy and mechanical behaviour. NATO ASI Series, vol. 213. Applied Sciences, 1992. p. 155.
[13] Yoo MH, Fu CL, Horton JA. Mater Sci Eng 1994;A176:431.
[14] Yoo MH, Fu CL. Mater Sci Eng 1992;A153:470.
[15] Yoo MH, Zou J, Fu, CL. Mater Sci Eng 1995;A192/193:14
[16] Stadler R, Podloucky R, Kresse G, Hafner J. Phys Rev 1998;B57:4088
[17] Fu CL. J Mater Res 1990;5:971.
[18] Yoo MH, Fu CL. Scr Metall Mater 1991;25:2345.
[19] Hong T, Smith JR, Srolovitz DJ, Gay JG, Richter R. Phys Rev B45:8775
[20] Banerjea A, Smith JR. Phys Rev B 1988;37:6632.
[21] Vinet P, Rose JH, Ferrante J, Smith JR. J Phys 1989;1:1941.
[22] Reynolds JE, Smith JR, Srolovitz DJ, Zhao G-L. In: Selinger RLB et al., editors. Fracture-instability dynamics, scaling, and ductile/brittle behavior. Symp. Proc., vol. 409. Pittsburgh (PA): MRS, 1996. p. 177–182.
[23] Gilman JJ. Fracture. Cambridge (MA): The MIT Press, 1959.
[24] Kelly A. Strong solids. Oxford: Clarendon Press, 1966.
[25] Macmillan NH, Kelly A. Mater Sci Eng 1972;10:139.
[26] Cherepanov GP. Mechanics of brittle fracture. New York: McGraw-Hill Int'l Book Co, 1979.
[27] Yoo MH. Scr Metall 1979;13:131.
[28] Simmons G, Wang H. Single crystals elastic constants and calculated aggregate properties: a handbook. 2nd ed. New York: John Wiley & Sons, 1971.
[29] Nakamura M. In: editors Intermetallic compounds, vol. 1, principles. Westbrook JH and Fleischer RL, New York: John Wiley & Sons, 1994. p. 873.
[30] Fu CL, Yoo MH. Acta Metall Mater 1992;40:703.
[31] Smith JR, Perry T, Banerjea A, Ferrante J, Bozzolo G. Phys Rev B 1991;44:6444.
[32] Daw MS. Phys Rev B 1989;39:7441.
[33] Finnis MW, Sinclair JE. Phil Mag A 1984;50:45.
[34] Cox H. Surface Sci 1998;397:374.
[35] Fu CL, Ye Y-Y, Yoo MH. Phil Mag Lett 1993;67:179
[36] Yoo MH, Fu CL. Metall Mater Trans A 1998;29:49.
[37] Fu CL, Yoo MH. Phil Mag Lett 1988;58:199.
[38] Mehl MJ, Klein BM, Papaconstantopoulos DA. In: Westbrook JH, Fleischer RL, editors. Intermetallic Compounds, vol. 1, Principles. John Wiley & Sons, 1994. p. 195.
[39] Ito K, Nakamoto T, Inui H, Yamaguchi M. In: Koch CC et al., editors. High-temperature ordered intermetallic alloys VII. Symp. Proc., vol. 460. Pittsburgh (PA): MRS, 1997. p. 599.
[40] Fu CL, Ohnishi S, Jansen HJF, Freeman AJ. Phys Rev B, 1985;31:1168.
[41] Wasilewski RJ, Trans. TMS-AIME, 1966;236:455.
[42] He Y, Schwarz RB, Darling T, Hundley M, Whang SH, Wang ZM. Mater Sci Eng 1997;A239–240:157.
[43] Rusovic, N. and Warlimont, H., Phys. Stat. Sol (a), 1977, 44, 609.
[44] Leamy HJ, Gibson ED, Kayser FX. Acta Met 1967;15:1827.
[45] Mathew JW, Phil Mag 1974;29:797.
[46] Yoo MH, Fu CL. In: Phillpot SR et al., editors. Microscopic simulation of interfacial phenomena in solids and liquids. Symp. Proc., vol. 492. Pittsburgh (PA): MRS, 1998. p. 345.
[47] Yoo MH, Fu CL. ISIJ International 1991;31:1049.
[48] Ludwig M, Gumbsch P. Acta Mater 1998;46:3135.
[49] Farkas D. In: Koch CC et al. High-temperature ordered intermetallic alloys VII. Symp. Proc., vol. 460. Pittsburgh (PA): MRS, 1997. p. 399.
[50] Foiles, Daw MS. J Mater Res 1967;2:5.
[51] Schneibel JH, Hazzledine PM. J Mater Res 1992;7:868.
[52] George EP, Porter WD, Joy DC. In: Liu CT et al., editors. High-temperature ordered intermetallic alloys III. Symp. Proc., vol. 133. Pittsburgh (PA): MRS, 1989. p. 311.
[53] Wu ZL, Pope DP. In: Darola R et al., editors. Structural intermetallics. Warrendale (PA): TMS, 1993. p. 107.
[54] Wade RK, Petrovic JJ. J Am Cer Soc 1992;75:1682.
[55] Peralta P, Maloy SA, Chu F, Petrovic JJ, Mitchell TE. Scr Mater 997;37:1599.